A LETTER submitted to *Limnology & Oceanography Letters*

DOC, Grazers and Resilience of Phytoplankton to Enrichment

Short title (37 characters): **DOC and resilience to enrichment**

by

Stephen R. Carpenter[1*], Michael L. Pace[2], and Grace M. Wilkinson[1]

[1]Center for Limnology, University of Wisconsin, Madison, WI 53706 USA

[2]Department of Environmental Sciences, University of Virginia, Charlottesville, Virginia 22904 USA

*Corresponding author: Steve.Carpenter@wisc.edu

Word count (Introduction, Methods, Results, Discussion = 3176 with 4 figures

Author Contribution Statement

All 3 authors conceived this synthesis, participated in the whole-lake experiments, and contributed to the writing.

Data Availability Statement

Original field data in the Environmental Data Initiative repository:

Carpenter, S., J. Kitchell, J. Cole, and M. Pace. 2017. Cascade Project at North Temperate Lakes LTER Core Data Carbon 1984 - 2016 ver 6. Environmental Data Initiative. https://doi.org/10.6073/pasta/8d71e8d3fdec619807e5c05fa1b3eb13.

Carpenter, S., J. Kitchell, J. Cole, and M. Pace. 2017. Cascade Project at North Temperate Lakes LTER Core Data Nutrients 1991 - 2016 ver 3. Environmental Data Initiative. https://doi.org/10.6073/pasta/f2956422d5797c61fe6ceb15faa19f3b.

Pace, M., J. Cole, and S. Carpenter. 2020. Cascade project at North Temperate Lakes LTER - Daily Chlorophyll Data for Whole Lake Nutrient Additions 2013-2015 ver 2. Environmental Data Initiative. https://doi.org/10.6073/pasta/d480f53082da7ea53e349183a0c8a714.

Pace, M., J. Cole, and S. Carpenter. 2020. Cascade project at North Temperate Lakes LTER - High Frequency Data for Whole Lake Nutrient Additions 2013-2015 ver 2. Environmental Data Initiative. https://doi.org/10.6073/pasta/cbe19041db41e720d84970f43156c042.

Calculated data and R scripts are available in GitHub distributed by Zenodo:

Carpenter, S.R. and B.M.S. Arani. 2021. Exit and survival time: New standard scripts. August 2021. Zenodo. https://doi.org/10.5281/zenodo.6544226

Carpenter, S.R. 2022. Eigenvalues of multivariate autoregression models versus time. Zenodo. https://doi.org/10.5281/zenodo.6522653

Carpenter, S.R. 2022. Chlorophyll dynamics: model of response to DOC, grazing, and phosphorus. Zenodo. https://doi.org/10.5281/zenodo.6568114

Carpenter, S.R. and M.L. Pace 2022. DOC, TP, TN of Peter and Tuesday Lakes, Unenriched Years 2003-2012. Zenodo, https://doi.org/10.5281/zenodo.6607788

Carpenter, S.R. and M.L. Pace. 2022. Prediction of mixed layer depth from DOC and phosphorus input rate. Zenodo. https://doi.org/10.5281/zenodo.6568103

Scientific Significance Statement (93 words)

Many lakes are undergoing simultaneous increases in light-absorbing dissolved organic carbon (DOC) and nutrients due to a combination of human activities in the watershed and climate change. Nutrient enrichment can result in algal blooms, or the critical transition from a low to high state of phytoplankton biomass. However, it is unclear if DOC alters the resilience of lakes undergoing nutrient enrichment. To understand this relationship, we evaluate resilience for experimentally enriched lakes with contrasting DOC. Resilience of phytoplankton to enrichment was increased by higher DOC in combination with thermocline depth and grazer biomass.

Abstract (149 words)

Phytoplankton blooms often follow nutrient enrichment. Differences among lakes in light-absorbing dissolved organic carbon (DOC) may shift bloom thresholds to higher nutrient loads and thereby increase resilience of lakes to enrichment. To explore this idea, we measured resilience to experimental enrichment of two lakes with contrasting DOC concentrations. We compared bloom thresholds in both lakes using a model of phytoplankton response to DOC and nutrients, a dynamic time series indicator of resilience, and two empirical measures of stochastic resilience, mean exit time and median survival time. For the dynamic indicator and ecosystem model the lake with higher DOC was more resilient to enrichment. However, the distributions overlapped for stochastic indicators of resilience of the two lakes. These analyses show that DOC interacts with mixing depth and zooplankton biomass to affect resilience. Strong contrasts in DOC and many observations are needed to discern effects of DOC on resilience to enrichment.

Keywords: chlorophyll, DOC, nutrients, phycocyanin, zooplankton, whole-lake experiment

Enrichment of lakes and reservoirs by excessive nutrient loads impairs water resources worldwide (Schindler 2012; Smith et al. 2006). Enrichment causes blooms of cyanobacteria, and consequences include hypoxia, mass mortality of fishes, and adverse effects on human health (Huisman et al. 2018; Isles and Pomati 2021). Blooms are characterized by a state of high phytoplankton biomass, which contrasts with an alternate state of low phytoplankton biomass. Transitions between states are shaped by the interaction of nutrient enrichment with grazers and physical properties of the water column (Isles et al. 2015; Kosten et al. 2012; Soranno 1997). The contrasting states are separated by an unstable threshold (Scheffer 2009). Each state is locally stable because equilibrium is restored after small disturbances. Large disturbances, however, may cause the ecosystem to cross the threshold to the alternate state (Carpenter et al. 2022).

Many lakes are simultaneously experiencing increases in water color and nutrient loading (Leech et al. 2018). Water color from chromophoric dissolved organic carbon (DOC) is mainly terrestrial in origin (Wilkinson et al. 2013) and concentrations change in response to hydrogeology, vegetation, and precipitation in the watershed (Carpenter and Pace 2018; Gergel et al. 1999; Zwart et al. 2016). Inputs of DOC affect stratification, phytoplankton growth, and response to nutrient enrichment by altering light and nutrient availability (Jones et al. 2005; Rinke et al. 2010; Solomon et al. 2015). Higher loads of DOC decreased stability of mesocosm food webs and increased their sensitivity to nutrient pulses (Jones and Lennon 2015). Terrestrial DOC is accompanied by nitrogen and phosphorus some of which supports phytoplankton growth (Corman et al. 2018; Kissman et al. 2017; Qualls et al. 1991). Primary production has a hump-shaped response to increasing DOC concentrations due to tradeoffs between nutrient

115 enhancement and shading effects (Kelly et al. 2018; Olson et al. 2020). This response seems
116 dependent on carbon-nutrient stoichiometry (Isles et al. 2021), and correlations of DOC, color,
117 and limiting nutrients are variable among watersheds and lakes (Lapierre et al. 2021; Stetler et al.
118 2021).
119
120 Resilience measures the tendency of a state, such as the low-phytoplankton state of a lake, to
121 persist despite changes in its environment, such as nutrient supply (Holling 1973). While
122 stability measures the rate of recovery from local perturbations (Ives and Carpenter 2007),
123 resilience considers effects of repeated and large disturbances, environmental trends, and the
124 possibility that the ecosystem could cross thresholds to alternate states (Holling 1996; Scheffer et
125 al. 2015). If the low-phytoplankton state is resilient to a specified nutrient input then it does not
126 cross the threshold to the high-phytoplankton state. Thus resilience is the response of a specified
127 state of the ecosystem to a specified environmental perturbation (Carpenter et al. 2001a).
128
129 Since DOC affects phytoplankton stability and response to nutrient enrichment, we hypothesized
130 that the resilience of phytoplankton to nutrient enrichment may depend on DOC. This study
131 compares resilience to nutrient enrichment of phytoplankton biomass in two experimental lakes
132 with contrasting DOC for which we have detailed data on phytoplankton response to enrichment
133 (Wilkinson et al. 2018). We apply three approaches to assess resilience: (1) a model of
134 chlorophyll responses to nutrient enrichment, DOC and grazers; (2) comparative resilience of
135 phytoplankton to experimental enrichment of two contrasting lakes while monitoring dynamic
136 indicators of resilience (Ives and Dakos 2012; Scheffer et al. 2015); and (3) comparisons of
137 stochastic resilience of the low-phytoplankton state to nutrient enrichment (Arani et al. 2021;

Carpenter et al. 2022). We find that higher DOC may increase resilience of chlorophyll to enrichment but this effect is complicated by thermocline depth, grazer biomass, and stochasticity.

Methods

Lake descriptions: Whole-lake enrichments were conducted on Peter and Tuesday Lakes located in Gogebic County, Michigan, USA (46°250 N, 89°500 W). Before enrichment Peter and Tuesday lakes had relatively low primary production (Carpenter et al. 2005; Carpenter and Kitchell 1993). Both lakes are surrounded by fringing bogs and hardwood-conifer forests. A third lake, Paul Lake, served as undisturbed reference ecosystem.

Although the lakes are less than 1 km apart they differ in some key limnological characteristics. Prior to this experiment we measured DOC, total phosphorus (TP), total nitrogen (TN) and their ratios during years with no enrichment, 2003-2012. Tuesday Lake had higher concentrations of DOC, TP, and TN during these unenriched years (Fig. S1).

During this study, the mean thermocline during summer stratification was deeper in Peter Lake (1.9 m) than in Tuesday Lake (1.2 m). DOC and chlorophyll mean summer concentrations were higher in Tuesday Lake (9.7 mg/L and 17.0 µg/L respectively) than in Peter Lake (5.4 mg/L and 7.9 µg/L). Zooplankton biomass was relatively low in Tuesday Lake (1.8 µg C/L) versus Peter Lake (12.2 µg/L) consistent with food web contrasts established during earlier ecosystem experiments (Carpenter et al. 2001b; Pace et al. 2013). Overall, nutrient concentrations in this

161 study and prior manipulations (Carpenter et al. 2001b) indicate phytoplankton limitation by
162 nutrients, particularly phosphorus.
163
164 *Limnological methods*: During 2013-2015 we made weekly measurements of dissolved organic
165 carbon (Carpenter et al. 2017a) and nutrients (Carpenter et al. 2017b). A portion of filtered water
166 sample was preserved with 200 µL of 1 mol/L H_2SO_4 per 20 mL of sample and analyzed for
167 DOC with a Shimadzu 5050 TOC analyzer (Shimadzu, Kyoto, Japan). Zooplankton biomass was
168 estimated daily in 2015 by duplicate daytime verticals tows of an 153 µm mesh conical net,
169 towed through the upper two-thirds of the water column over the deepest point of the lake
170 Zooplankton samples were concentrated onto pre-weighted filters, dried, and re-weighted to
171 determine biomass (Pace et al. 2013).
172
173 Phycocyanin, dissolved oxygen, and pH were measured at 5-minute intervals using Hydrolab
174 DS5X sensors (OTT Hydromet, Loveland, Colorado, USA) sensors suspended at a depth of 0.75
175 m from a centrally-located buoy in Paul, Peter, and Tuesday lakes (Pace et al. 2020b). Daily
176 phycocyanin was the mean sensor value between 2200 to 0400 to avoid quenching (Rousso et al.
177 2021). Daily ranges (maximum – minimum for each day) were calculated for dissolved oxygen
178 saturation and pH. A manual sample for chlorophyll analysis was taken near the buoy each day
179 between 1000 and noon and stored in a dark cooler. The sample was filtered (pore size = 0.7 µm)
180 and extracts from the filters were analyzed fluorometrically for chlorophyll a concentration
181 (Holm-Hansen 1978; (Pace et al. 2020a). We used thermistor chains with temperature sensors
182 every half meter. The 5-minute temperatures were averaged to daily values to determine mixed
183 layer depth.Nutrient additions were made by dissolving ammonium nitrate (NH_4NO_3) and

184 phosphoric acid (H_3PO_4) in ~20 L of lake water and then distributing the mixture into the
185 epilimnion of each lake in the propeller wash of an underway electric motor. Nutrient additions
186 occurred between 11:00 and 13:00 daily. Descriptions of enrichments for 2013-2015 are
187 presented by Wilkinson et al. (2018).
188
189 *Overview of stability and resilience analyses*: We report three analyses of stability and resilience
190 for two enriched lakes with contrasting DOC: (1) analysis of a model of phytoplankton response
191 to DOC, grazers and enrichment fit to daily data from 2015, (2) multivariate time series analysis
192 of daily data during 2015 to determine the time of transition from a low-phytoplankton state to a
193 high-phytoplankton state, and (3) calculation of two indices of stochastic resilience, mean exit
194 time and median survival time, using high-frequency data from 2013-2015. Below we
195 summarize each resilience method and then the data used for the analyses.
196
197 *Model of Phytoplankton Response to DOC and Enrichment:* We developed a simple ecosystem
198 model to assess DOC and enrichment effects on phytoplankton (S.I. *Phytoplankton response to*
199 *DOC, Enrichment, and Grazing*). Daily observed time series were phytoplankton concentration
200 A (µg C/L), zooplankton biomass H (µg C L^{-1}), DOC concentration C (mg/L), and thermocline
201 depth Z_T (m) (Fig. S3). C, A and Z_T are necessary to estimate m, the mean irradiance in the
202 mixed layer using extinction coefficients measured for these lakes. A is measured as chlorophyll
203 concentration (µg/L) and converted to carbon units (µg/L) using the measured C:Chl mass ratio
204 of 60 (Carpenter et al. 2016). For model projections the time step Δt was 0.1 d. We fit the model
205 to data and calculated one-step projections using the difference equation (S.11):
206

$$A_{t+1} = A_t + \left\{ rmA_t\left(1 - \frac{A_t}{pP}\right) - \frac{h_{max} H A_t^q}{v^q + A_t^q} e^{-bA_t} \right\} \Delta t + \varepsilon_t \qquad [1]$$

DOC affects growth through mean irradiance in the mixed layer m (S.I. equations S1-S4) and daily P load (P) determines phytoplankton carrying capacity through parameter p. The model rationale, parameter definitions and estimates, and methods of stability analysis are presented in S.I. *Phytoplankton response to DOC, Enrichment, and Grazing*.

Effect of DOC on Thermocline Depth: The model of phytoplankton response to DOC, nutrients, and grazing requires an equation to predict thermocline depth from DOC and P load rate. Thermocline depth affects the phytoplankton model through the mean irradiance of the mixed layer (eq. S4 – S6) and dilution of areal P loads to calculate P concentration. We estimated the effect of DOC, P load rate, and lake fetch on depth of the thermocline by regression analysis of 8 nearby lakes for years between 1999 and 2016 when all variates were measured between 15 July and 15 August (S.I. *Estimating Thermocline Depth from Lake Area, DOC and P Load*).

Time series indicators of resilience:

We assessed stability at each daily time step of 2015 using multivariate time series models (Ives and Dakos 2012) estimated by Bayesian updating (Pole et al. 1994). Multivariate time series models (eq. S13 – S15) were fit to daily series of four observed variates (Fig. S4): log10 phycocyanin, log10 chlorophyll *a*, delta dissolved oxygen saturation (daily maximum – daily minimum), and delta pH (daily maximum – daily minimum. Models are described in S.I. *Multivariate time series analysis to assess stability* and worked examples with data and R scripts are presented by Carpenter et al. (2022).

Stochastic Resilience: We computed mean exit time and median survival time (Arani et al. 2021) to measure stochastic resilience. Mean exit time from a state is the mean time until the ecosystem crosses the threshold to an alternate state, and median survival time is the median time that the ecosystem occupies a specified state. Stochastic resilience accounts for the random fluctuations of the data, whereas resilience indicators from the multivariate time series analysis and fits of the ecosystem model provide point estimates of the threshold. For details of the calculations see S.I. *Stochastic Measures of Resilience*.

Data for analyses: The phytoplankton model and multivariate time series analysis used daily observations from 2015 (Pace et al. 2020a) including chlorophyll concentration, zooplankton biomass, mixed layer depth, and DOC. 2015 was the only enriched year with daily zooplankton biomass data needed for the phytoplankton model. During 2015, daily enrichments to Peter and Tuesday lakes were identical (3 mg P m^{-2} d^{-1} with N:P ratio 15:1) starting on day of year 152. In 2015, Peter bloomed earlier and enrichment was ended on day 180 (Pace et al. 2017). Tuesday bloomed later in the summer and enrichment ended on day 240 (Wilkinson et al. 2018).

High-frequency measurements of phycocyanin from all three enriched years (Pace et al. 2020b) were used to compute stochastic resilience (exit time) because of the large number of observations required by the method (Carpenter et al. 2022).

252 Results

253 *Phytoplankton Model*

254 The phytoplankton model uses chlorophyll to indicate biomass because we have extensive data
255 for the light extinction coefficient of chlorophyll (Carpenter et al. 1998). Nonetheless chlorophyll
256 and phycocyanin are highly correlated at the daily scale of the dynamic model (Fig S8; for Peter
257 Lake r = 0.944, Tuesday Lake r = 0.891) indicating the importance of Cyanobacteria in the
258 observed blooms. Covariates (DOC, thermocline depth, and zooplankton biomass) appear in
259 (Fig. S2).

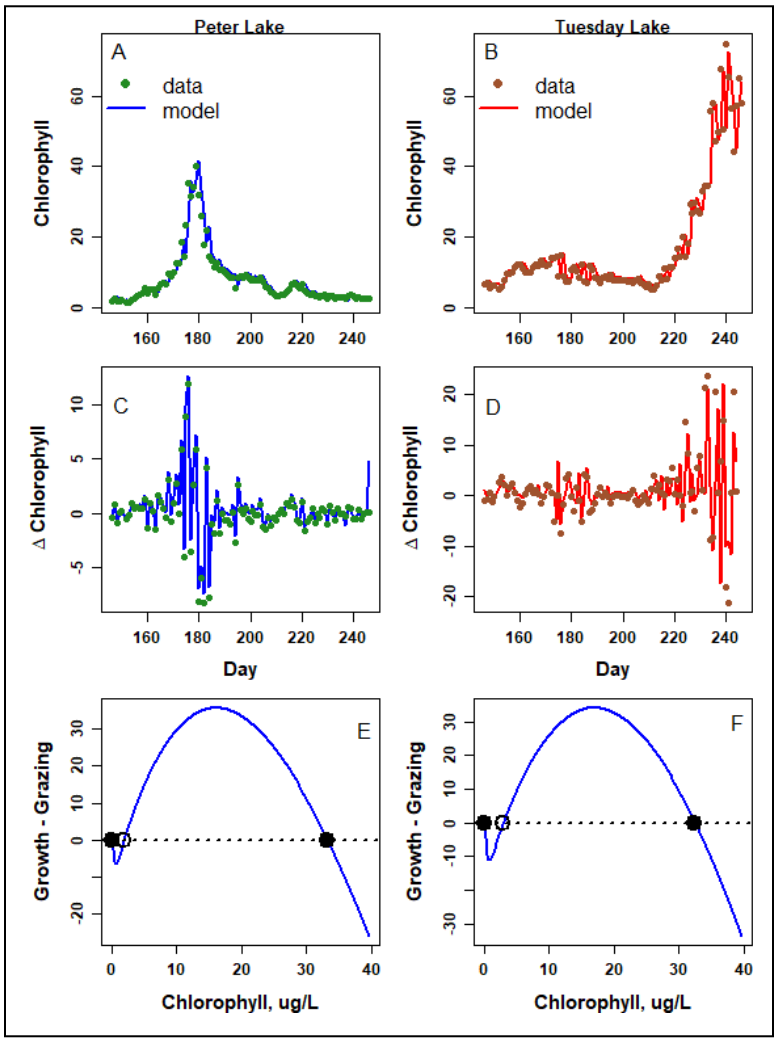

274 Figure 1. Time series of predictions (solid line) and observations (solid circles) of chlorophyll (ug/L) versus day number of 2015 for (A) Peter Lake and (B) Tuesday Lake. Time series of predicted one-day change in chlorophyll () for (C) Peter Lake and (D) Tuesday Lake. Plots of net growth rate versus chlorophyll concentration for (E) Peter Lake and (F) Tuesday Lake. Filled circles are stable equilibria and open circles are unstable equilibria.

275

One-day predictions of chlorophyll concentration track the observations (Fig. 1A, B) and time series of predicted and observed one-day change in chlorophyll are similar (Fig. 1C, D). The largest differences in predicted and observed one-step change, and the greatest variability, occur near the unstable thresholds (approximately day 175 in Peter Lake and day 219 in Tuesday Lake). Analyses of residuals are presented in S.I. *Phytoplankton response to DOC, Enrichment, and Grazing*.

Model predictions are consistent with alternate states for conditions that we have observed in each lake (Fig. 1 E, F). The net growth line of each panel crosses zero at 3 points, stable equilibria at low and high phytoplankton biomass and an intermediate unstable threshold.

We used the model to compare effects of DOC and zooplankton biomass on the critical threshold for daily phosphorus load. The critical P load to a given lake is the lowest P load where a high-pigment equilibrium appears. At the critical P load a single low equilibrium for chlorophyll concentration transitions to three equilibria. The calculation of the critical threshold for P load required a regression model to predict thermocline depth from DOC and P load (S.I. *Estimating Thermocline Depth from Lake Area, DOC, and P Load*). For specified values of DOC, zooplankton biomass, and thermocline depth the critical threshold for P load is calculated from the phytoplankton model (S.I. *Equilibria and Critical Points*).

Using Peter Lake as an example thermocline depth decreases as DOC and P load increase (Fig. 2A). Thermocline depths are within the range observed for Peter Lake (Fig. S2). Critical P load increases slightly with DOC for constant zooplankton biomass (Fig. 2B). In contrast the critical P load increases substantially with zooplankton biomass for constant DOC (Fig. 2B).

299 Figure 2. Contour plots of (A) thermocline depth versus DOC (mg L^{-1}) and P load rate

300 (mg P m^{-2} d^{-1}) and (B) critical P load rate versus DOC and zooplankton biomass (mg C m^{-3}) for

301 the area of Peter Lake.

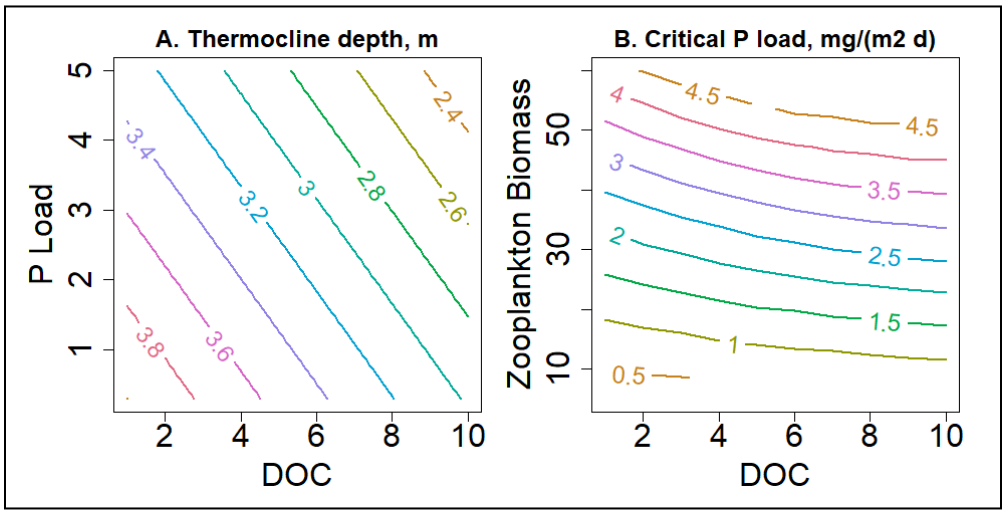

309

310

Multivariate time series analyses

Stability and loss of stability were estimated daily from the parameter matrix of multivariate time series models (S.I. *Multivariate time series analysis to assess stability*). Modulus of the maximum eigenvalue indicates stability if the eigenvalue is less than 1, or loss of stability when the eigenvalue exceeds 1 (Fig. 3). The unenriched reference lake, Paul Lake, had eigenvalues below 1 and appeared to be stable throughout 2015 (Fig. 3A). Peter Lake (Fig. 3B) was destabilized on day 175, with Cyanobacterial blooms apparent by day 170 (Pace et al. 2017; Wilkinson et al. 2018). Although Tuesday Lake received an identical nutrient load, the first indication of instability occurred 44 days later on day 219 (Fig. 3C). Cyanophytes dominated during the blooms in both lakes in 2015 (Wilkinson et al. 2018).

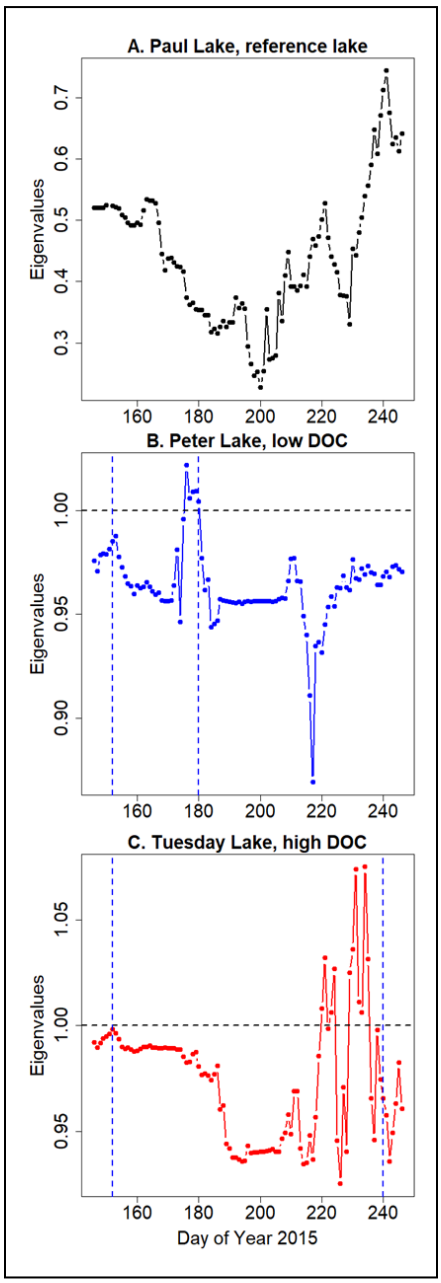

Figure 3. Largest eigenvalue of interaction matrix versus day of year 2015 in (A) Paul, (B) Peter and (C) Tuesday lakes. Vertical dashed lines indicate the start and end of enrichment with identical daily loads of inorganic P and N. Eigenvalues > 1 (horizontal dashed line) indicate critical transition between low and high pigment states.

335 *Stochastic Resilience*

336 Stochastic indicators of resilience show no consistent differences between Peter and Tuesday
337 lakes (Fig. 4). Resilience to enrichment is illustrated by mean exit time and median survival time
338 of the low-pigment state (Fig. 4A,C). For the low pigment basin, Peter Lake has slightly shorter
339 mean exit time but slightly longer survival time. This difference may reflect the greater influence
340 of extreme values on the mean than the median. Resilience of the Cyanobacterial bloom is
341 illustrated by mean exit time and median survival time of the high-pigment state (Fig. 4B, D).
342 Peter Lake has shorter mean exit time and slightly shorter median survival time, suggesting that
343 the bloom of Peter Lake is less resilient than that of Tuesday Lake. The relatively pronounced
344 shift of the mean suggests a stronger influence of extreme fluctuations in Peter Lake.

345

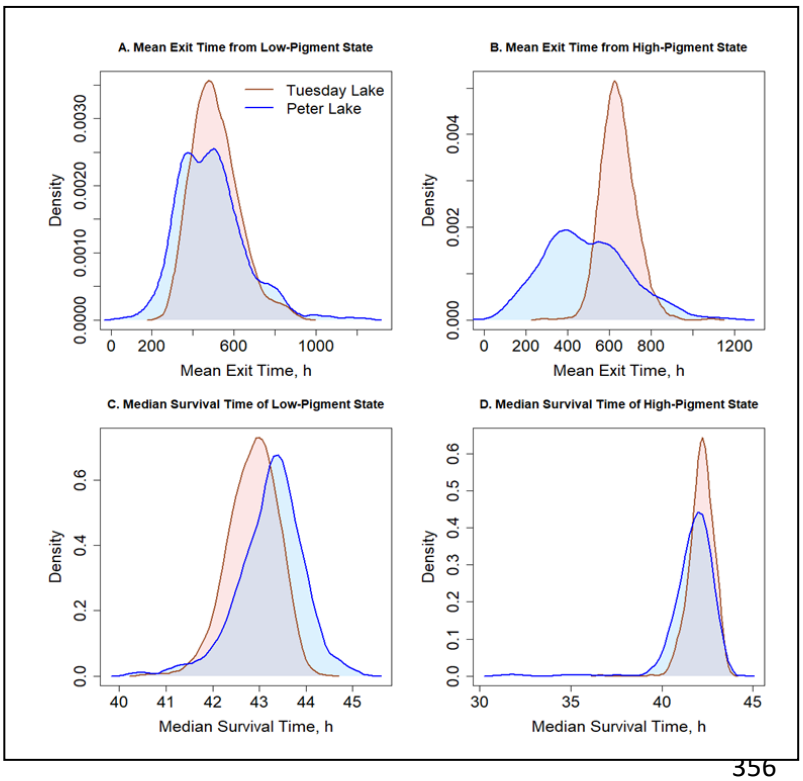

Fig. 4. Density plots for Peter and Tuesday lakes of (A) mean exit time from low-pigment state, (B) mean exit time from high-pigment state, (C) median survival time of low-pigment state, and (D) median survival time of high-pigment state. Each distribution is calculated from 1000 bootstrap samples.

356

357

358

359 Discussion

360

361 The ecosystem model fitted to the data tracks the delayed bloom in Tuesday Lake (Fig. 1).
362 Analysis of the fitted model suggests that the critical P load, an indicator of resilience, rises
363 steeply with zooplankton biomass and weakly with DOC (Fig. 2B).

364

365 The multivariate time series analysis shows that, under constant and equal rates of enrichment,
366 Peter Lake was destabilized 44 days before Tuesday Lake (Fig. 1). This contrast shows greater
367 resilience of Tuesday Lake to enrichment. However, the lakes differed in DOC, thermocline
368 depth, and zooplankton biomass and perhaps other dimensions. Given these differences, we
369 cannot conclude that higher DOC concentrations caused the higher resilience of Tuesday Lake,
370 but it is a possible mechanism for the difference in resilience.

371

372 The multivariate time series analysis (Fig. 3) and the critical P load (Fig. 2) provide point
373 estimates of resilience. These indicators show declining resilience and mark the time of critical
374 transition but do not account for the shape of the stability basin or the chance that a random
375 shock may knock the ecosystem over the threshold (Scheffer et al. 2015). Stochastic indicators
376 of resilience use the random fluctuations of the ecosystem to sample the stability basins and
377 thereby reconstruct their shape from a large sample of data (Arani et al. 2021). This more
378 complete analysis revealed a more complex picture (Fig. 4). Differences in resilience to
379 enrichment and resilience of the Cyanobacterial bloom are sensitive to random events, and
380 differences between the lakes are smaller than their ranges of variability.

381

Due to the large number of observations required to compute the stochastic indicators of resilience, we used the high-frequency sensor data from all three years of nutrient enrichments. During 2013-2015 Tuesday Lake had higher DOC but zooplankton biomass, thermocline depth, nutrient enrichment rates and weather fluctuated in each lake each year (Pace et al. 2019; Wilkinson et al. 2018). This variation potentially contributed to overlap in stochastic resilience of the lakes. More frequent pigment measurements (e.g. each minute) could have allowed calculations of stochastic resilience during 2015 alone (Arani et al. 2021), providing a comparison of the stability landscapes under constant enrichment.

Lakes are exposed to multiple, interacting stressors including eutrophication and brownification (Leech et al. 2018). Using a set of enrichment experiments in lakes with contrasting DOC and other factors, we showed that DOC may affect influence resilience but the effect is complicated by thermocline depth, grazer biomass, and randomness. Further whole-lake experiments are needed to assess the effects of DOC on resilience to enrichment. High-frequency datasets can be collected from a greater diversity of lakes, leading to comparison of stability landscapes under different conditions. A direct manipulation of DOC while collecting high-frequency data before, during, and after the change in DOC is needed as a direct test of the effect of DOC on resilience of phytoplankton. Such studies would lead to a broader understanding of the factors that affect lake ecosystem resilience to enrichment.

Acknowledgements: The National Science Foundation supported the field research through DEB awards 1144624 and 1144683 to SRC and MLP. SRC's work on the paper was partially

supported by NSF through DEB 1754712 and 1753854 and a Hilldale Award from University of Wisconsin-Madison.

REFERENCES

Arani, B. M. S., S. R. Carpenter, L. Lahti, E. H. van Nes, and M. Scheffer. 2021. Exit time as a measure of ecological resilience. Science **372:** eaay4895.10.1126/science.aay4895

Carpenter, S., B. Walker, J. M. Anderies, and N. Abel. 2001a. From Metaphor to Measurement: Resilience of What to What? Ecosystems **4:** 765-781.10.1007/s10021-001-0045-9

Carpenter, S. R. 2022. Eigenvalues of multivariate autoregression models versus time. Zenodo.https://doi.org/10.5281/zenodo.6522653

Carpenter, S. R., B. M. S. Arani, E. H. Van Nes, M. Scheffer, and M. L. Pace. 2022. Resilience of phytoplankton dynamics to trophic cascades and nutrient enrichment. Limnology and Oceanography **67:** S258-S265.https://doi.org/10.1002/lno.11913

Carpenter, S. R. and others 2001b. Trophic cascades, nutrients and lake productivity: Whole-lake experiments. Ecological Monographs **71:** 163-186.doi:10.1890/0012-9615(2001)071[0163:TCNALP]2.0.CO;2

Carpenter, S. R., J. J. Cole, J. F. Kitchell, and M. L. Pace. 1998. Impact of dissolved organic carbon, phosphorus and grazing on phytoplankton biomass and production in lakes. Limnology and Oceanography **43:** 73-80.

Carpenter, S. R. and others 2005. Ecosystem subsidies: Terrestrial support of aquatic food webs from 13C addition to contrasting lakes. Ecology **86:** 2737-2750.https://doi.org/10.1890/04-1282

426 Carpenter, S. R., J. J. Cole, M. L. Pace, and G. M. Wilkinson. 2016. Response of plankton to
427 nutrients, planktivory and terrestrial organic matter: a model analysis of whole-lake
428 experiments. Ecology Letters **19:** 230-239.10.1111/ele.12558
429 Carpenter, S. R., and J. F. Kitchell [eds.]. 1993. Trophic Cascades in Lakes. Cambridge
430 University Press.
431 Carpenter, S. R., J. F. Kitchell, J. J. Cole, and L. Pace Michael. 2017a. Cascade Project at North
432 Temperate Lakes LTER Core Data Carbon 1984-2016. Environmental Data
433 Initiative.https://doi.org/10.6073/pasta/8d71e8d3fdec619807e5c05fa1b3eb13
434 ---. 2017b. Cascade Project at North Temperate Lakes LTER: Core Data Nutrients 1991-2016.
435 Environmental Data
436 Initiative.https://doi.org/10.6073/pasta/f2956422d5797c61fe6ceb15faa19f3b
437 Carpenter, S. R., and M. L. Pace. 2018. Synthesis of a 33-yr series of whole-lake experiments:
438 Effects of nutrients, grazers, and precipitation-driven water color on chlorophyll.
439 Limnology and Oceanography Letters **3:** 419-427.doi:10.1002/lol2.10094
440 Corman, J. R., B. L. Bertolet, N. J. Casson, S. D. Sebestyen, R. K. Kolka, and E. H. Stanley.
441 2018. Nitrogen and Phosphorus Loads to Temperate Seepage Lakes Associated With
442 Allochthonous Dissolved Organic Carbon Loads. Geophysical Research Letters **45:**
443 5481-5490.https://doi.org/10.1029/2018GL077219
444 Gergel, S. E., M. G. Turner, and T. K. Kratz. 1999. DISSOLVED ORGANIC CARBON AS AN
445 INDICATOR OF THE SCALE OF WATERSHED INFLUENCE ON LAKES AND
446 RIVERS. Ecological Applications **9:** 1377-1390.https://doi.org/10.1890/1051-
447 0761(1999)009[1377:DOCAAI]2.0.CO;2

448 Holling, C. S. 1973. Resilience and Stability of Ecological Systems. Annual Review of Ecology
449 and Systematics **4:** 1-23.10.1146/annurev.es.04.110173.000245
450 ---. 1996. Engineering resilience versus ecological resilience, p. 31-44. *In* National Academy of
451 Engineering [ed.], Engineering Within Ecological Constraints. National Academies Press.
452 Huisman, J., G. A. Codd, H. W. Paerl, B. W. Ibelings, J. M. H. Verspagen, and P. M. Visser.
453 2018. Cyanobacterial blooms. Nature Reviews Microbiology **16:** 471-
454 483.10.1038/s41579-018-0040-1
455 Isles, P. D., and F. Pomati. 2021. An operational framework for defining and forecasting
456 phytoplankton blooms. Frontiers in Ecology and the Environment **19:** 443-
457 450.https://doi.org/10.1002/fee.2376
458 Isles, P. D. F., I. F. Creed, A. Jonsson, and A.-K. Bergström. 2021. Trade-offs Between Light
459 and Nutrient Availability Across Gradients of Dissolved Organic Carbon Lead to
460 Spatially and Temporally Variable Responses of Lake Phytoplankton Biomass to
461 Browning. Ecosystems **24:** 1837-1852.10.1007/s10021-021-00619-7
462 Isles, P. D. F., C. D. Giles, T. A. Gearhart, Y. Xu, G. K. Druschel, and A. W. Schroth. 2015.
463 Dynamic internal drivers of a historically severe cyanobacteria bloom in Lake Champlain
464 revealed through comprehensive monitoring. Journal of Great Lakes Research **41:** 818-
465 829.https://doi.org/10.1016/j.jglr.2015.06.006
466 Ives, A. R., and S. R. Carpenter. 2007. Stability and Diversity of Ecosystems. Science **317:** 58-
467 62.10.1126/science.1133258
468 Ives, A. R., and V. Dakos. 2012. Detecting dynamical changes in nonlinear time series using
469 locally linear state-space models. Ecosphere **3:** art58.10.1890/es11-00347.1

Jones, I., G. George, and C. S. Reynolds. 2005. Quantifying effects of phytoplankton on the heat budgets of two large limnetic enclosures. Freshwater Biology **50:** 1239-1247.https://doi.org/10.1111/j.1365-2427.2005.01397.x

Jones, S. E., and J. T. Lennon. 2015. A test of the subsidy–stability hypothesis: the effects of terrestrial carbon in aquatic ecosystems. Ecology **96:** 1550-1560.https://doi.org/10.1890/14-1783.1

Kelly, P. T., M. J. González, W. H. Renwick, and M. J. Vanni. 2018. Increased light availability and nutrient cycling by fish provide resilience against reversing eutrophication in an agriculturally impacted reservoir. Limnology and Oceanography **63:** 2647-2660.doi:10.1002/lno.10966

Kissman, C. E. H., C. E. Williamson, K. C. Rose, and J. E. Saros. 2017. Nutrients associated with terrestrial dissolved organic matter drive changes in zooplankton:phytoplankton biomass ratios in an alpine lake. Freshwater Biology **62:** 40-51.https://doi.org/10.1111/fwb.12847

Kosten, S. and others 2012. Warmer climates boost cyanobacterial dominance in shallow lakes. Global Change Biology **18:** 118-126.10.1111/j.1365-2486.2011.02488.x

Lapierre, J.-F., S. M. Collins, S. K. Oliver, E. H. Stanley, and T. Wagner. 2021. Inconsistent browning of northeastern U.S. lakes despite increased precipitation and recovery from acidification. Ecosphere **12:** e03415.https://doi.org/10.1002/ecs2.3415

Leech, D. M., A. I. Pollard, S. G. Labou, and S. E. Hampton. 2018. Fewer blue lakes and more murky lakes across the continental U.S.: Implications for planktonic food webs. Limnology and Oceanography **63:** 2661-2680.doi:10.1002/lno.10967

492 Olson, C. R., C. T. Solomon, and S. E. Jones. 2020. Shifting limitation of primary production:
493 experimental support for a new model in lake ecosystems. Ecology Letters **23:** 1800-
494 1808.https://doi.org/10.1111/ele.13606
495 Pace, M. L. and others 2017. Reversal of a cyanobacterial bloom in response to early warnings.
496 Proceedings of the National Academy of Sciences **114:** 352-
497 357.10.1073/pnas.1612424114
498 Pace, M. L., S. R. Carpenter, R. A. Johnson, and J. T. Kurzweil. 2013. Zooplankton provide
499 early warnings of a regime shift in a whole-lake manipulation. Limnology and
500 Oceanography **58:** 525-532.
501 Pace, M. L., S. R. Carpenter, and G. M. Wilkinson. 2019. Long-term studies and reproducibility:
502 Lessons from whole-lake experiments. Limnology and Oceanography **64:** S22-
503 S33.doi:10.1002/lno.11012
504 Pace, M. L., J. J. Cole, and S. R. Carpenter. 2020a. Cascade project at North Temperate Lakes
505 LTER - Daily Chlorophyll Data for Whole Lake Nutrient Additions 2013-2015
506 Environmental Data
507 Initiative.https://doi.org/10.6073/pasta/d480f53082da7ea53e349183a0c8a714
508 Pace, M. L., J. J. Cole, and S. R. Carpenter. 2020b. Cascade project at North Temperate Lakes
509 LTER - High Frequency Data for Whole Lake Nutrient Additions 2013-2015
510 Environmental Data
511 Initiative.https://doi.org/10.6073/pasta/cbe19041db41e720d84970f43156c042
512 Pole, A., M. West, and J. Harrison. 1994. Applied Bayesian forecasting and time series analysis.
513 Chapman & Hall.

514 Qualls, R. G., B. L. Haines, and W. T. Swank. 1991. Fluxes of Dissolved Organic Nutrients and
515 Humic Substances in a Deciduous Forest. Ecology **72:** 254-266.10.2307/1938919
516 Rinke, K., P. Yeates, and K. O. Rothhaupt. 2010. A simulation study of the feedback of
517 phytoplankton on thermal structure via light extinction. Freshwater Biology **55:** 1674-
518 1693.https://doi.org/10.1111/j.1365-2427.2010.02401.x
519 Rousso, B. Z., E. Bertone, R. A. Stewart, K. Rinke, and D. P. Hamilton. 2021. Light-induced
520 fluorescence quenching leads to errors in sensor measurements of phytoplankton
521 chlorophyll and phycocyanin. Water Research **198:**
522 117133.https://doi.org/10.1016/j.watres.2021.117133
523 Scheffer, M. 2009. Critical transitions in nature and society. Princeton University Press.
524 Scheffer, M., S. R. Carpenter, V. Dakos, and E. H. van Nes. 2015. Generic Indicators of
525 Ecological Resilience: Inferring the Chance of a Critical Transition. Annual Review of
526 Ecology, Evolution, and Systematics **46:** 145-167.doi:10.1146/annurev-ecolsys-112414-
527 054242
528 Schindler, D. W. 2012. The dilemma of controlling cultural eutrophication of lakes. Proceedings
529 of the Royal Society B: Biological Sciences **279:** 4322-4333.10.1098/rspb.2012.1032
530 Smith, V. H., S. B. Joye, and R. W. Howarth. 2006. Eutrophication of freshwater and marine
531 ecosystems. Limnology and Oceanography **51:** 351-355.
532 Solomon, C. T. and others 2015. Ecosystem Consequences of Changing Inputs of Terrestrial
533 Dissolved Organic Matter to Lakes: Current Knowledge and Future Challenges.
534 Ecosystems **18:** 376-389.10.1007/s10021-015-9848-y

535 Soranno, P. A. 1997. Factors affecting the timing of surface scums and epilimnetic blooms of
536 blue-green algae in a eutrophic lake. Canadian Journal of Fisheries and Aquatic Sciences
537 **54:** 1965-1975.10.1139/f97-104
538 Stetler, J. T., L. B. Knoll, C. T. Driscoll, and K. C. Rose. 2021. Lake browning generates a
539 spatiotemporal mismatch between dissolved organic carbon and limiting nutrients.
540 Limnology and Oceanography Letters **6:** 182-191.https://doi.org/10.1002/lol2.10194
541 Wilkinson, G. M. and others 2018. Early warning signals precede cyanobacterial blooms in
542 multiple whole-lake experiments. Ecological Monographs **88:** 188-
543 203.doi:10.1002/ecm.1286
544 Wilkinson, G. M., M. L. Pace, and J. J. Cole. 2013. Terrestrial dominance of organic matter in
545 north temperate lakes. Global Biogeochem Cy **27:** 43-51.10.1029/2012gb004453
546 Zwart, J. A. and others 2016. Metabolic and physiochemical responses to a whole-lake
547 experimental increase in dissolved organic carbon in a north-temperate lake. Limnology
548 and Oceanography **61:** 723-734.doi:10.1002/lno.10248

549

Supporting Information
for
DOC, Grazers, and Resilience of Phytoplankton to Enrichment
by
Stephen R. Carpenter[1*], Michael L. Pace[2], and Grace M. Wilkinson[1]

[1]Center for Limnology, University of Wisconsin, Madison, WI 53706 USA
*Correspondence: Steve.Carpenter@wisc.edu

[2]Department of Environmental Sciences, University of Virginia, Charlottesville, Virginia 22904 USA

Contents

DOC and Nutrients in Peter and Paul Lakes Prior to Enrichment

DOC, TP, TN, and their ratios were calculated for years prior to enrichment, 2003-2012 (Fig. S1) from datasets posted online (Carpenter et al. 2017a; Carpenter et al. 2017b). Means and confidence intervals were calculated for all samples at and above the depth where irradiance was 25% of surface irradiance. Data and R scripts for Fig. S1 are available online (Carpenter and Pace 2022a).

Fig. S1. DOC and nutrients during summer stratification in epilimnions of Peter and Tuesday lakes during 2003–2012, prior to the nutrient enrichment experiments. Error bars are 95% confidence intervals. N = 236 for Peter Lake and N = 26 for Tuesday Lake.

Upper row: DOC, TP, and TN. Lower row: Ratios (by mass).

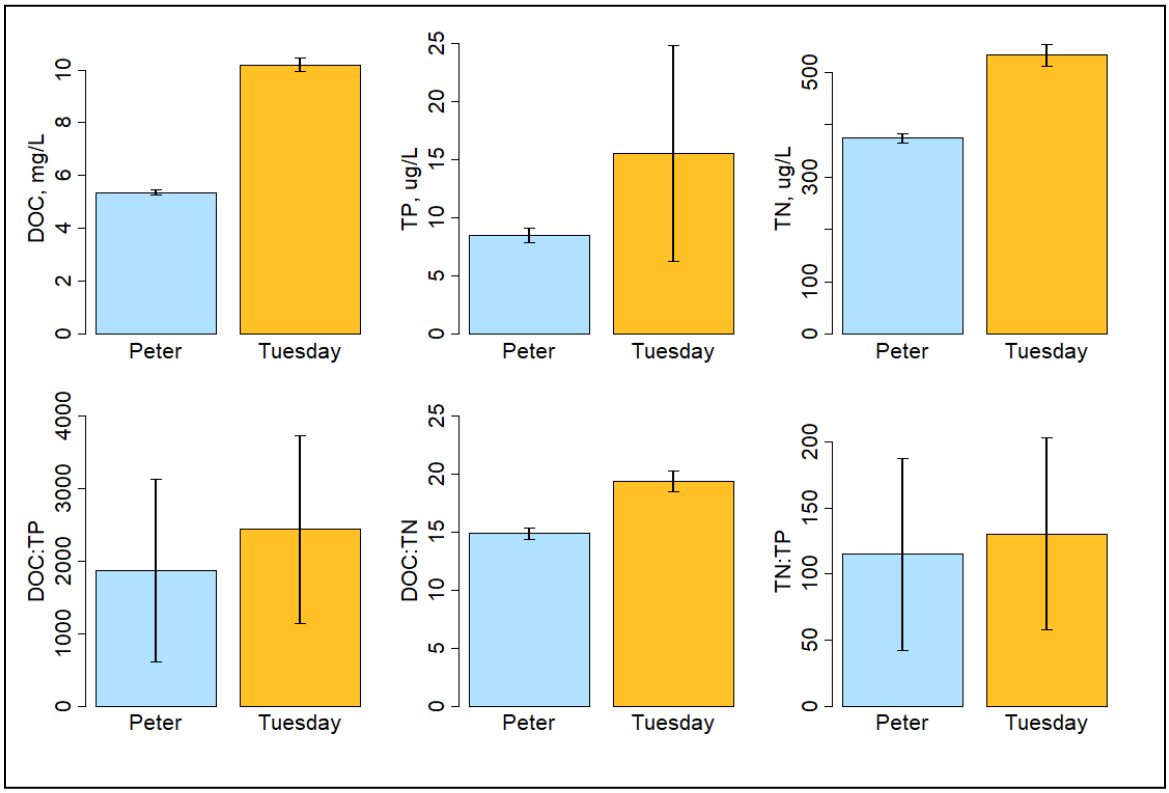

Phytoplankton Response to DOC, Enrichment and Grazers

We developed a model of phytoplankton response to fluctuations of DOC, P load and grazing during the whole-lake experiments. We focus on phytoplankton dynamics in the mixed layer (as chlorophyll mg m^{-3} and carbon mg C m^{-3} converted with the observed C-to-Chl ratio of 60) (Carpenter et al. 2016) (Fig. S2).

Figure S2. Daily time series of variates used to fit the model of phytoplankton biomass responses to DOC, P load, and zooplankton grazing during 2015 in Peter and Tuesday lakes (left and right columns respectively). Variates (rows) are chlorophyll (µg/L), zooplankton biomass (µg C/L), DOC (mg/L) and mixed layer depth (m).

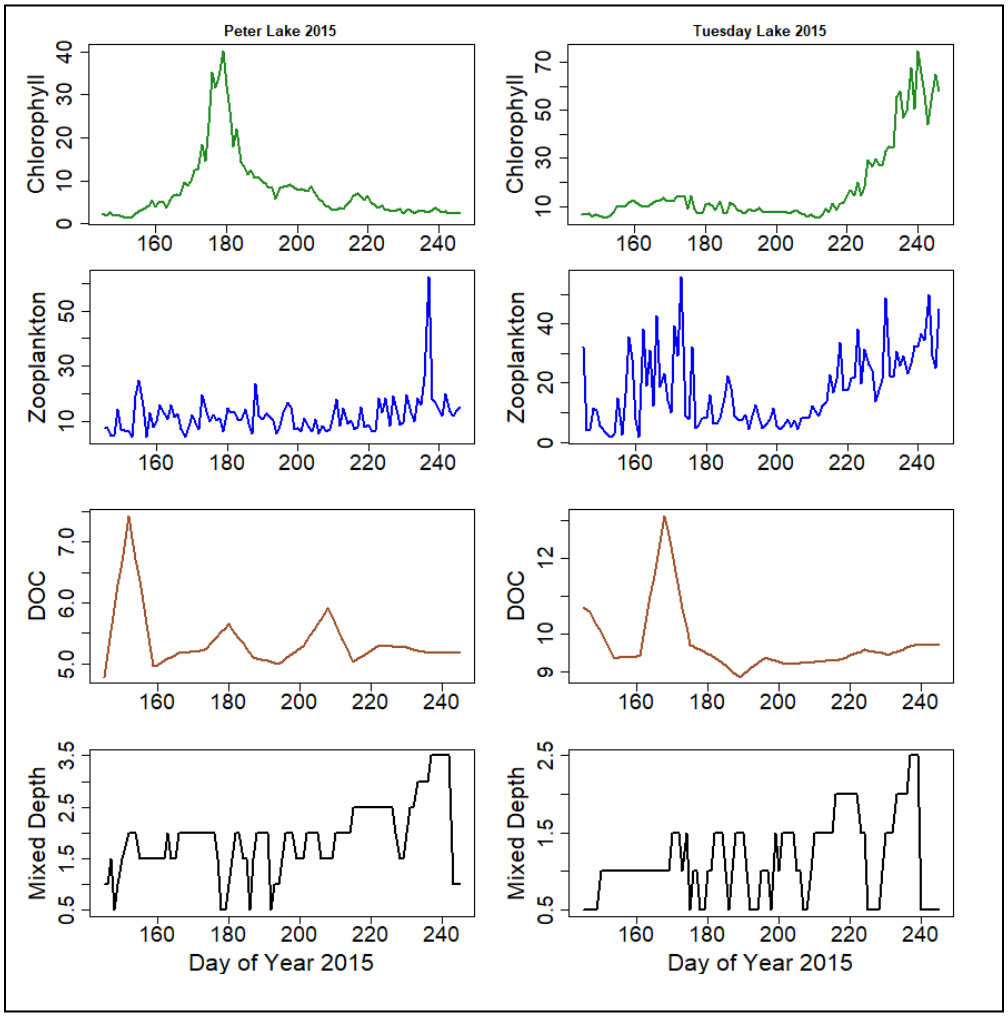

Irradiance and shading by phytoplankton and DOC

The irradiance in the mixed layer depends on light absorption by DOC (C) and phytoplankton (A). The shading coefficient for depth z $= -\phi_W z - \phi_C C z - \phi_A A z$ where the ϕ are extinction coefficients for water, DOC, and chlorophyll measured directly in these lakes (Carpenter et al. 1998).

The mean irradiance in the mixed layer $\mu(z_T)$ over thermocline depth z_T with surface irradiance I_0 is found using the Beer-Lambert law with pooled solutes with light absorption coefficient $k = \phi_W + \phi_C C + \phi_A A$:

$$\mu(z_T) = \frac{1}{z_T}\int_0^{z_T} I_0 e^{-kz} dz \qquad [S.4]$$

Completing the integral:

$$\mu(z_T) = \frac{I_0}{z_T}\left[c + \frac{e^{-kZ}}{-k}\right]|_0^{z_T} = \frac{I_0}{z_T}\left[\left(c - \frac{1}{k}e^{-kz_T}\right) - \left(c - \frac{1}{k}e^{0}\right)\right] \qquad [S.5]$$

Simplifying the algebra:

$$\mu(z_T) = \frac{I_0}{z_T}\frac{1}{k}[1 - e^{-kz_T}] \qquad [S.6]$$

Phytoplankton dynamics

To construct a dynamic model for phytoplankton we assume that DOC and grazer biomass (which affects grazing loss rate) change slowly compared to phytoplankton biomass. Further we assume that irradiance affects phytoplankton growth rate (r below) and cumulative phosphorus enrichment affects maximum phytoplankton biomass (K below). We cannot assess nitrogen effects on phytoplankton because N and P were added at a fixed ratio and not varied independently. Experience shows that dissolved inorganic P concentration is usually not detectable due to rapid uptake by phytoplankton (while dissolved inorganic N accumulates). Thus all of the available P is in phytoplankton and we base the model on P-limitation of phytoplankton. However at high phytoplankton biomass the phytoplankton are limited by shading not nutrients and dissolved inorganic P may be measurable (Carpenter and Lathrop 2014; Carpenter et al. 2001).

We assume that mean irradiance affects r and that P enrichment affects K. K = pP where p is a positive constant and P is the current P enrichment rate in mg P m^{-2} d^{-1}. We set p = 1/5 where 5 mg P m^{-2} d^{-1} was the loading rate associated with high sustained summer chlorophyll concentration of 60 mg m^{-3} (Carpenter et al. 2001).

The dynamics of phytoplankton biomass (as carbon concentration in the mixed layer) follow:

$$dA/dt = rmA - cA^2 - G \qquad [S.7]$$

including growth r·m where m = μ(z_T), the mean mixed layer irradiance defined above, competition $c = rm / pP$ where p and P are defined above, and grazing loss G. As an example, for algal A growth without grazing the equilibria dA/dt = 0 are A = 0 and A = rm/c = K by the definition of carrying capacity (Scheffer et al. 2008).

G is a grazing function of A and herbivore biomass H:

$$G = \frac{h_{max} H A^q}{v^q + A^q} e^{-bA} \qquad [S.8]$$

with maximum rate h_{max} and half-saturation v. The coefficient b accounts for reduced grazing rate at high phytoplankton biomass due to interference with the grazing mechanism (Scheffer et al. 2008)

Collecting terms, the model is:

$$dA/dt = rmA - \frac{rmA^2}{pP} - \frac{h_{max} H A^q}{v^q + A^q} e^{-bA} \qquad [S.9]$$

where m is mean light intensity in the mixed layer given by [S.7].

In conventional logistic form the model is

$$dA/dt = rmA\left(1 - \frac{A}{pP}\right) - \frac{h_{max} H A^q}{v^q + A^q} e^{-bA} \qquad [S.10]$$

To calculate one-step projections and link the model to data, phytoplankton dynamics of equation S.10 were rewritten in discrete form with one-step error ε_t:

$$A_{t+1} = A_t + \left\{ rmA_t\left(1 - \frac{A_t}{pP}\right) - \frac{h_{max} H A_t^q}{v^q + A_t^q} e^{-bA_t} \right\} \Delta t + \varepsilon_t \qquad [S.11]$$

We set surface irradiance to 600 μE m-2 s-1, a typical summer value (Carpenter et al. 2016). The mean irradiance in the mixed layer m was calculated from DOC and chlorophyll concentrations using extinction coefficients measured by Carpenter et al. (1998) (equations S4 – S7). The grazing half-saturation parameter v (18 μg C/L) was based on mass-balance estimates of grazing loss (Carpenter et al. 2016). The rate parameters r (0.147 d^{-1}) and h_{max} (1.06 L mg^{-1}C) and model error σ(ε_t) (4.18 mg C L^{-1}) were estimated by minimizing the negative log likelihood of ε_t (Hilborn and Mangel 1997). The grazing exponent q = 2, the classical value for the type-III functional response, had lower negative log likelihood than the discrete alternatives 1 or 3. The interference coefficient for grazing at high algal biomass was 10^{-4} (Scheffer et al. 2008).

Data of Fig. S2 and R scripts for fitting the model and calculating equilibria and critical values of P load are available online (Carpenter 2022b).

Model Residuals

Time series of one-step predictions of chlorophyll and daily change in chlorophyll are shown in main text Figure 1. The model fit has lower negative log likelihood by 2.3 units compared to a null model A(t) = A(t+1).

Observed chlorophyll concentration is plotted against predictions and residuals in Fig. S3. Residuals are larger at higher chlorophyll concentrations.

Figure S3. Left: Predicted versus observed chlorophyll (µg/L). Note log-log axes. Right: Predicted chlorophyll versus residuals. Note log x-axis.

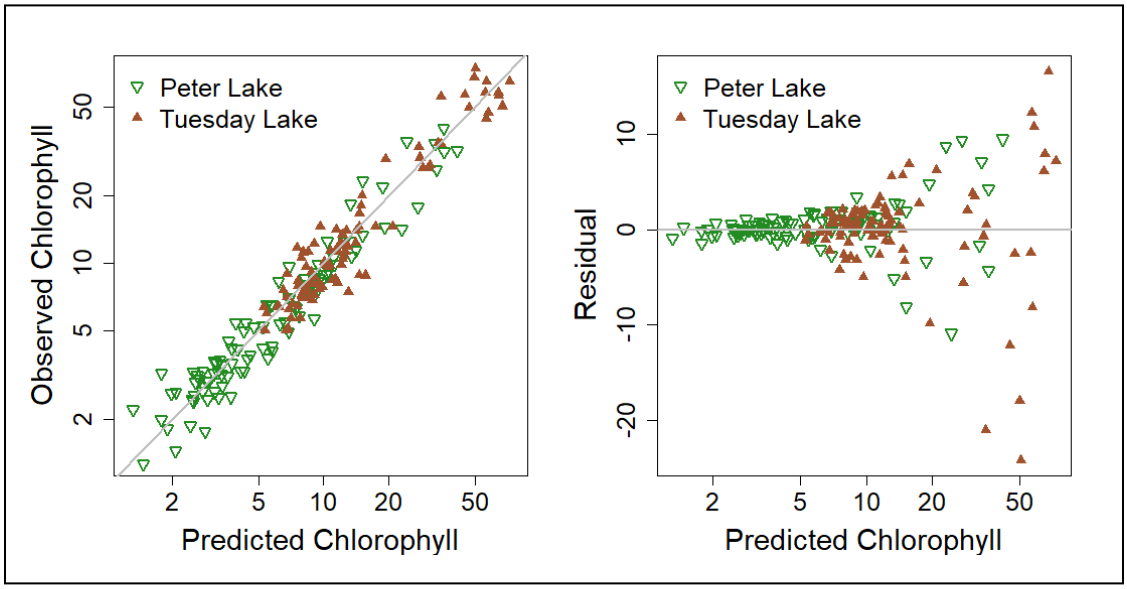

Residuals are nearly uncorrelated (Fig. S.4A, B) and the original data are highly autocorrelated (Fig. S4C,D).

Figure S4. Autocorrelation functions for residuals (A,B) and observed chlorophyll (C,D).

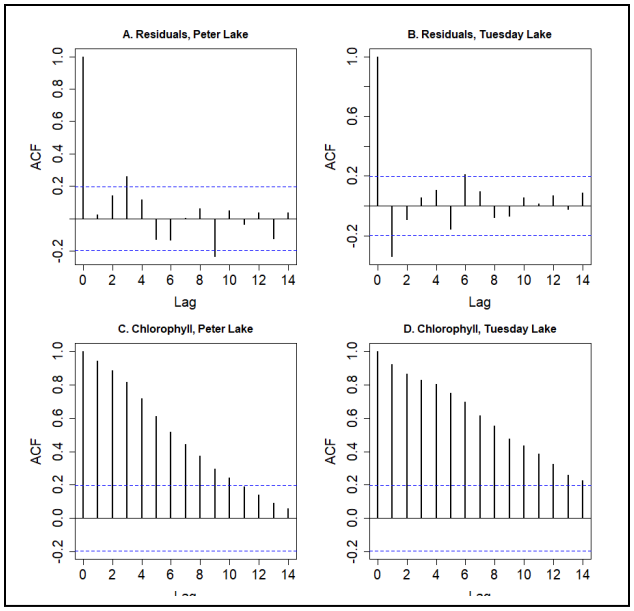

Residuals show no notable trends versus covariates (Figs. S5, S6). When plotted versus day of 2015 (Fig. S5 and S6 top left) residuals are larger in magnitude at the times that the unstable threshold was reached.

Figure S5. Model residuals for Peter Lake versus day of 2015, DOC, thermocline depth, and zooplankton biomass.

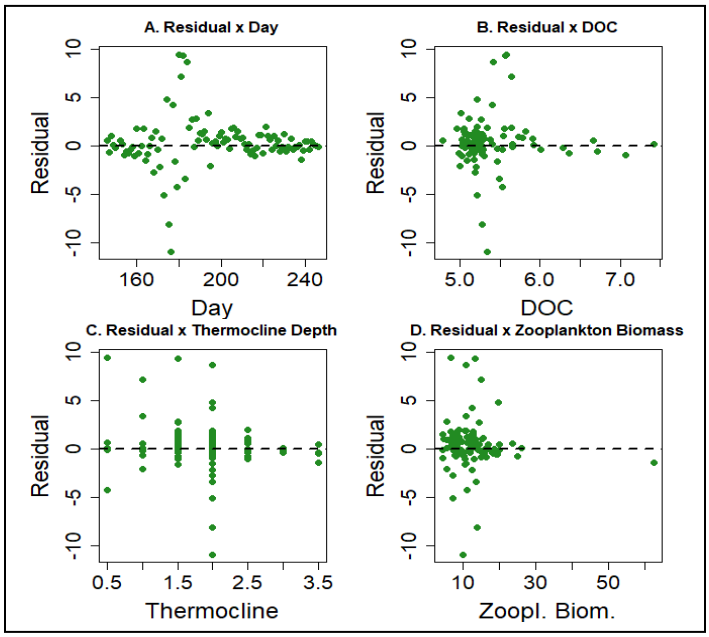

Figure S6. Model residuals for Tuesday Lake versus day of 2015, DOC, thermocline depth, and zooplankton biomass.

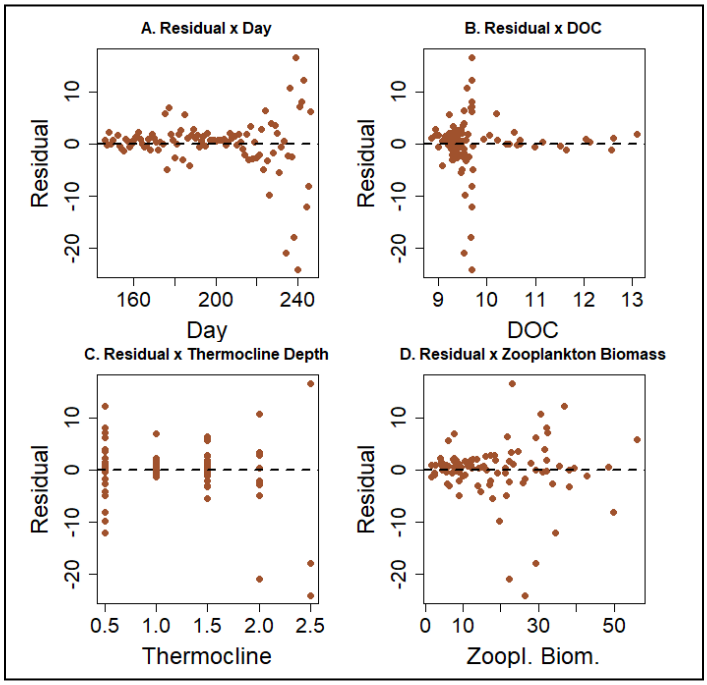

Estimating Thermocline Depth from Lake Area, DOC and P Load

We fit an empirical model to estimate thermocline depth from DOC and daily P load rate. The regression model was needed to calculate equilibria of the phytoplankton model, including critical transitions points, as a function of DOC, P load rate, and grazer biomass. We regressed Zmix (thermocline depth in m) on DOC (mg L^{-1}), P load rate (mg P m^{-2} d^{-1}), and square root of lake area (m), an index of average fetch using data from Paul, Peter, and Tuesday lakes as well as 5 neighboring lakes we studied in previous years (Carpenter and Pace 2018): Crampton, East Long, Hummingbird, Ward, and West Long.

Square root of lake area was included as a covariate because the 8 lakes vary more than thirty-fold in area. However model results reported in the main text (Fig. 2) use observed mixed layer depths (Fig. S2).

We analyzed means of Zmix, DOC, and P load for dates between 15 July and 15 August in each available year for each lake. We used these late-summer dates to minimize effects of seasonality and transients of manipulations.

The fitted regression is presented in Table S1 with residual plots in Figure S7. Data and the R scripts are provided online (Carpenter and Pace 2022b).

Table S1. Regression model to predict Zmix as a linear function of intercept, square root of lake area, DOC, and P load. Residual standard error was 0.41 m on 82 degrees of freedom with adjusted $R^2 = 0.733$. For DOC and P load effects $p < 10^{-9}$. The $area^{0.5}$ effect has $p = 0.0369$ after accounting for the smaller error degrees of freedom among 8 lakes.

Independent variate	**Estimate**	**Standard Error**
Intercept	3.53	0.147
$Area^{0.5}$	0.00692	0.00010
DOC	-0.114	0.012
P load	-0.151	0.032

Larger lakes have longer fetch, indexed by square root of area, and deeper thermocline depth. Thermocline depth became shallower with increasing DOC and P load, consistent with an effect of light extinction as reported previously by Kling (1988). Other research has shown that phytoplankton biomass affects the depth and strength of stratification (Jones et al. 2005) and thermal dynamics of the water column (Rinke et al. 2010).

Residual plots show no discernible bias (patterns that suggest additional model terms)(Draper and Smith 1981) and residuals are consistent with a normal distribution (Fig. S7).

Fig. S7. Residual plots of errors from the regression in Table S1. Starting from top left, panels show: observed versus predicted thermocline depth with solid blue 1:1 line; normal QQ plot (normal probability plot) with solid blue line where Normal distribution matches the observed distribution; scatterplots of residuals versus DOC and square root of lake area.

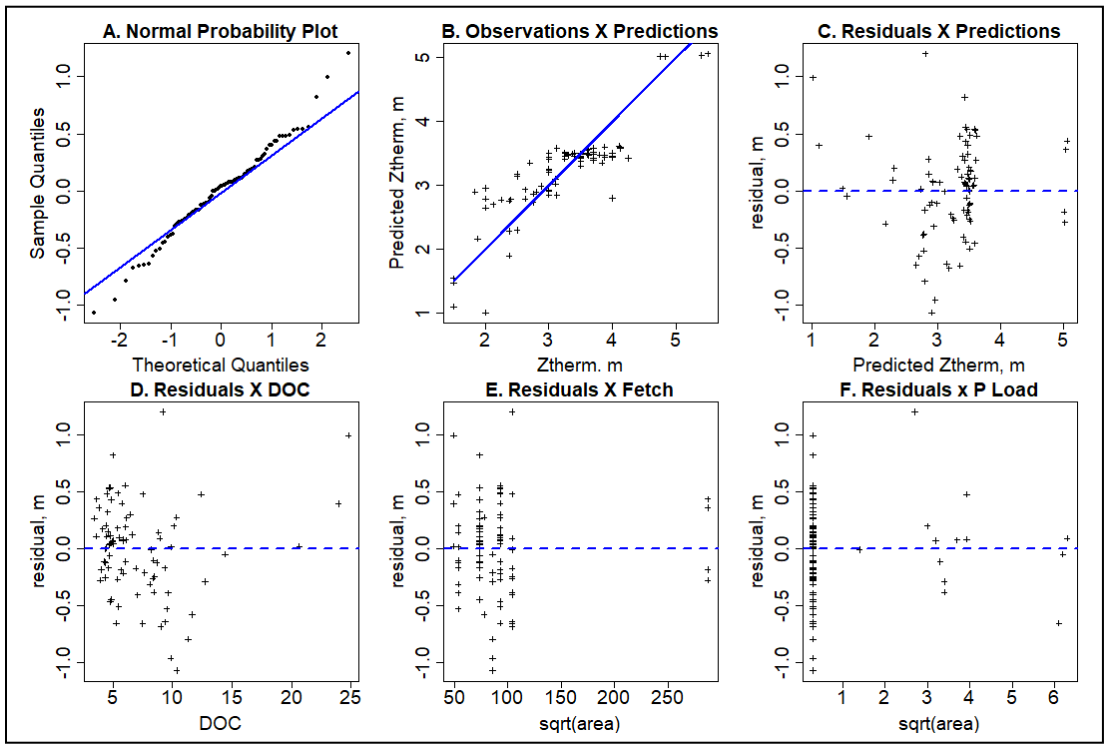

Equilibria and critical points

Equilibria of S.11 are values of A where $A_{t+1} = A_t$, hence the bracketed rate function f(A) is zero:

$$f(A) = \left\{ rmA_t \left(1 - \frac{A_t}{pP}\right) - \frac{h_{max} H A_t^q}{v^q + A_t^q} e^{-bA_t} \right\} \qquad [S.12]$$

We found equilibria numerically by solving f(A) = 0 using Brent's method in the optim() function of R 4.1.1.

The critical transition between low- and high-biomass states occurs at a value of A where f(A) = 0 and df(A)/dA = 0. The critical point depends on DOC (which affects mixed layer depth and mean irradiance in the mixed layer, m, through S.6), grazer biomass H, and enrichment rate P. For fixed values of DOC and H, we found the critical values of A and P by solving simultaneously for f(A) = 0 and df(A)/dA = 0 using the Nelder-Mead method in the optim() function of R 4.1.1. The derivative df(A)/dA was computed using small (± 1%) increments and decrements of A. To check critical values of P we also computed equilibria along a gradient of P values and then found the lowest P value where the system switched from one to three equilibria.

The R script for fitting and analyzing the model (Carpenter 2022b) includes code for finding the equilibria and critical point.

Multivariate time series analysis to assess stability

When an ecosystem arrives at an unstable threshold the net rate of change approaches zero and variance increases rapidly (Scheffer et al. 2015). The appearance of a threshold in time series data can be determined by fitting time-varying autoregressions (equations S1 – S3). If the ecosystem data are generated by a nonlinear multivariate stochastic process, then the linearization of that process around an equilibrium is a multivariate autoregression with time-varying parameters, as shown by Ives et al. (2003) equations 11 and 12 on p. 305 of their paper. The stability of the multivariate autoregression at any time point is given by the modulus of largest eigenvalue of the parameter matrix (Ives and Dakos 2012). In a stable region this modulus is smaller than 1. At an unstable threshold the modulus reaches or exceeds 1. Because parameters are updated at each time step we constructed a time series of eigenvalues (as modulus) and measured the resilience as the amount of time, or amount of P load, required to reach the unstable threshold (Ives and Dakos 2012).

We applied the method to assess stability each day of 2015. Eigenvalues of a multivariate autoregressive time series model are calculated at each time step. Stability is indicated by the eigenvalue of largest modulus (dominant eigenvalue) at each step. When the dominant eigenvalue is less than 1 then the system is stable. When the dominant eigenvalue reaches or exceeds 1 then the system has reached or crossed a threshold (Ives and Dakos 2012).

The multivariate autoregressive model in state-space form includes a data or observation equation

$$y_{t+1} = b_t + \phi_t y_t + \varepsilon_t \qquad [S.13]$$

where y_t the 4-element vector of observed variates at time t, b_t is the 4-element vector time series of the intercept or level parameter, ϕ_t is the 4x4 matrix of autoregressive parameters at time t, and ε_t is the 4-element vector time series of observation errors. The four variates observed daily were log10 phycocyanin, chlorophyll *a*, delta DOsat (daily maximum – daily minimum), and delta pH (daily maximum – daily minimum) (Fig. S8). Under nutrient enrichment of these lakes, large pH variation occurs over 24 hours due to net uptake of dissolved inorganic carbon during photosynthesis and net release of dissolved inorganic carbon during night respiration (Bade and Cole 2006).

The evolution of parameters over time follows the system equations, one for each parameter

$$b_t = b_{t-1} + \omega_{b,t-1} \qquad [S.14]$$
$$\phi_t = \phi_{t-1} + \omega_{\phi,t-1} \qquad [S.15]$$

Where $\omega_{b,t-1}$ is the 4-element vector time series of process errors in the level vector b_t, and $\omega_{\varphi,t-1}$ is the 4x4 matrix time series of process errors in the autoregression coefficient matrix ϕ. The observation errors and the process errors are multivariate Normal processes independent of each other and over time. Using prior distributions for initial values, the full model was estimated sequentially from the data by Bayesian updating (West and Harrison 1989) using the algorithm presented by Pole et al. (1994). Eigenvalues were computed using the 4x4 matrix of autoregression coefficients ϕ_t at each time step and the modulus of the largest eigenvalue was taken as the indicator of stability for that time step (Ives and Dakos 2012). For these datasets (Fig. 3) the eigenvalues were real (not complex) numbers.

The R script and the dataset to generate the time series of eigenvalues Fig. 3 from the time series in Fig. S8 are available online (Carpenter 2022c).

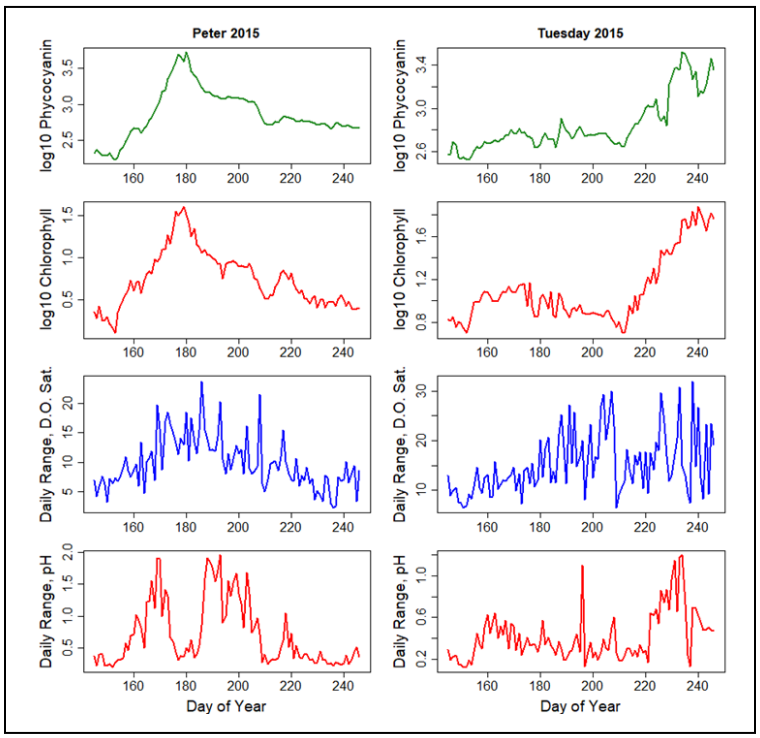

Figure S8. Indicators of response to enrichment versus day of year 2015 in Peter and Tuesday lakes: log10 of phycocyanin RFU measured each night between 2200 and 0400; log10 of chlorophyll measured by fluorometric analysis in the laboratory of a sample collected from the epilimnion at mid-day; daily range (maximum – minimum) of dissolved oxygen saturation; and daily range of pH.

Stochastic Measures of Resilience

We computed mean exit time as a measure of stochastic resilience (Arani et al. 2021) for both lakes using high-frequency phycocyanin time series data measured every 5 minutes during summer stratified seasons of 2013-2015 (Wilkinson et al. 2018). It was necessary to use all 3 years of data because precise estimation of mean exit time requires a large sample (Arani et al. 2021).

Peter and Tuesday lakes, like other bistable ecosystems, have alternate stable states separated by an unstable threshold. In this case the alternate states have low versus high concentrations of phycocyanin, a characteristic pigment of Cyanobacteria, and occasionally cross the threshold between states. An exit event occurs each time that the ecosystem crosses the unstable threshold, and the time lag between two exit events is a single realization of exit time. Mean exit time is the average exit time over the estimated stochasticity of exit times. The distribution of mean exit times over the data can be estimated by bootstrap sampling.

The procedure for estimating mean exit time, testing assumptions of stationarity and Markovicity, and bootstrapping the distribution over the data of mean exit times is explained in detail in the S.I. of Arani et al. (2021) and Carpenter et al. (2022). Data, R scripts, and step-by-step instructions are posted online (Carpenter and Arani 2021; Pace et al. 2020). An abbreviated summary is presented here.

We first standardized the time series of phycocyanin relative fluorescence units as levels $b_t/s(b_t)$ of the univariate autoregression equation S.13, where b_t is given by equation S.14 and $s(b_t)$ is the standard deviation of $\omega_{b,t}$ (eq. S.15). The standardized data are approximately stationary

according to the Augmented Dickey-Fuller (ADF) test, function adf.test() in the tseries library of R.

In addition to stationarity the standardized data should have the Markov property, i.e. each observation depends only on the previous observation. We could not reject the Markov hypothesis ($p < 0.01$) using the Box-Ljung and Rank tests in the spgs library of R. As a further test of the Markov property we estimated the Markov-Einstein time scale using the Chapman-Kolmogorov equation (Tabar 2019) calculated by the Matlab program provided by Arani et al. (2021). The Markov-Einstein time scale should be 1. For our data the estimates were less than 5. Although these data are near-Markov we still followed the Langevin approach (below) since it is likely more appropriate than advanced reconstruction schemes intended to account for colored noise (Hassanibesheli et al. 2020).

Nonparametric regression of the first and second moments of dx on x, where x is the time series of standardized levels defined above, is used to fit a drift-diffusion model known as the Langevin equation

$$dx = D_1(x)dt + \sqrt{2D_2(x)}\, dW \qquad \text{[S.16]}$$

(Carpenter and Brock 2011; Rinn et al. 2016; Tabar 2019). One-step changes (dx) that cross between years were not used in further analysis, although their effect on mean exit time and median survival time is trivial. In these equations x is the dynamic variable, t is time, and dW is a Weiner stochastic process. The function $D_1(x)$ or 'drift' is the deterministic core of the model. The function $D_2(x)$ or 'diffusion' is the stochastic variance of the model. The potential, stationary distribution, and exit times presented in Figs. S.9 and S.10 are computed from the drift and diffusion functions.

The potential function or 'ball and cup' diagram of ecology textbooks, with hills and valleys corresponding to stable and unstable regions respectively, is the integral of the drift function over x plotted against x. We instead present 'effective potential' which is appropriate when D_2 is not constant with x (Arani et al. 2021), as seen in our data (below). The effective potential U_f is

$$U_f(x) = \log D_2(\mathrm{x}) - \int_{xmin}^{x} \frac{D_1(y)}{D_2(y)} dy \qquad \text{[S.17]}$$

Here y is a dummy variable and xmin is the smallest observed value of x.

The stationary probability distribution is the probability distribution of the fitted Langevin equation at stationarity, i.e. after simulating the equation for infinite time. The stationary probability distribution can be calculated as

$$p_{st}(x) \propto \frac{1}{D_2(x)} \exp\left[\int_{xmin}^{x} \frac{D_1(y)}{D_2(y)} dy\right] \qquad \text{[S.18]}$$

(Arani et al. 2021). Our R code (Carpenter and Arani 2021) uses the hcubature() function of the cubature library in R to integrate the Fokker-Planck equation directly. The code follows Horsthemke and Lefever (1984) pages 110-111 as coded in Matlab by Carpenter and Brock (2006). We found that the curves generated by the two methods are nearly identical, and equation S.18 is easier to code and faster to compute When S.18 is used then a normalization factor is found by integrating $p_{st}(x)$ over the full range of x.

Mean exit time $T(x_0)$ is the average time it takes for particles starting at x_0 to exit a basin of attraction. In our case 'exit' means crossing the unstable threshold to the other basin. Writing x for x0 to simplify notation, T(x) is the solution of a boundary value problem (Arani et al. 2021; Gardiner 2009)

$$D_1(x)\frac{\partial T(x)}{\partial x} + D_2(x)\frac{\partial^2 T(x)}{\partial x^2} = -1 \qquad [S.19]$$

The boundary value problem is solved separately for each basin. In each basin the absorbing boundary (i.e. where T(x) = 0) is the unstable threshold value of x and the reflecting boundary (i.e. where $\frac{\partial T(x)}{\partial x} = 0$) is a plausible value of x near the range limit of the observed data. We solved eq. S.19 using the bvptwp() function of the bvpSolve package in R (Carpenter and Arani 2021).

After solving for mean exit time as a function of x, T(x), and the stationary distribution as a function of x, $p_{st}(x)$, the weighted mean exit time over an entire basin is found as the weighted average of T(x) where the weights are $p_{st}(x)$, following eq. S.24 of Arani et al. (2021).

Survival time is found by solving the survival equation for the survival function $S(t,x_0)$ where x_0 is a starting value of x (Arani et al. 2021; Tabar 2019). Writing $S(t,x_0)$ as simply S and x_0 as simply x for notational convenience the survival equation

$$\frac{\partial S}{\partial t} = D1(x)\frac{\partial S}{\partial x} + D2(x)\frac{\partial^2 S}{\partial x^2} \qquad [S.20]$$

with boundary conditions $S(0,x_0) = 1$. We solved eq. S.20 using the ode.1D() function of the deSolve library in R. The median survival time is defined as $S(T_{med}(x_0),x_0) = 0.5$ and calculated directly from the solution of the survival equation. R scripts to fit D1 and D2 and then compute mean weighted exit time and median survival time are provided online (Carpenter and Arani 2021).

Calculations of mean exit time for Peter and Tuesday lakes are presented in Figures S9 and S10. In all panels the x-axis is standardized level $b_t/s(b_t)$ of phycocyanin relative fluorescence units, where b_t is given by equation S.2 and $s(b_t)$ is the standard deviation of $\omega_{b,t}$.

Panels S9A and S10A show the time series that were analyzed.

Panels S9B and S10B present the drift functions, or deterministic core of the dynamics estimated by nonparametric regression of the time series. Equilibria occur where a drift function crosses the zero line.

Panels S9C and S10C show the stochasticity of the dynamics estimated by nonparametric regression of the time series. Diffusion is plotted as $\sqrt{2D_2(x)}$ to have the same units as D1.

Panels S9D and S9D show the effective potential, or stability landscapes for each lake. Valleys represent stable regions and hilltops are unstable.

Panels S9E and S10E present the stationary probability densities for each lake. These densities show that each lake spends most of the time in a stable valley.

Panels S9F and S10F show the exit time curves for each attractor in each lake. Exits, or transitions between attractors, occur when the stochastic path of the ecosystem crosses the critical threshold, an unstable equilibrium. Mean exit time is the probability-weighted mean over the x-axis range of an attractor where weights are the stationary probability densities.

Uncertainties of mean exit times were computed by bootstrapping from the data following the procedure of Carpenter et al. (2022) for 1000 cycles. Bootstrap frequency distributions of mean exit times are presented in the main text. An example with R code is posted online (Carpenter 2022a).

Figure S.9 (left) and S.10 (right). Resilience analysis of Peter Lake (left column) and Tuesday Lake (right column) during 2013-2015. For each lake the panels are (A) Phycocyanin (standardized level) versus year during the experiment. Solid horizontal line denotes the unstable equilibrium. (B) Drift function versus phycocyanin standardized level showing stable equilibria (solid dots) and critical threshold (open circle). (C) Diffusion function versus phycocyanin standardized level. (D) Effective potential versus phycocyanin standardized level. (E) Stationary probability density versus phycocyanin standardized level. (F) Exit time (hours) versus phycocyanin standardized level, with probability-weighted means, for the two stable basins. Vertical dotted line is the threshold between the basins.

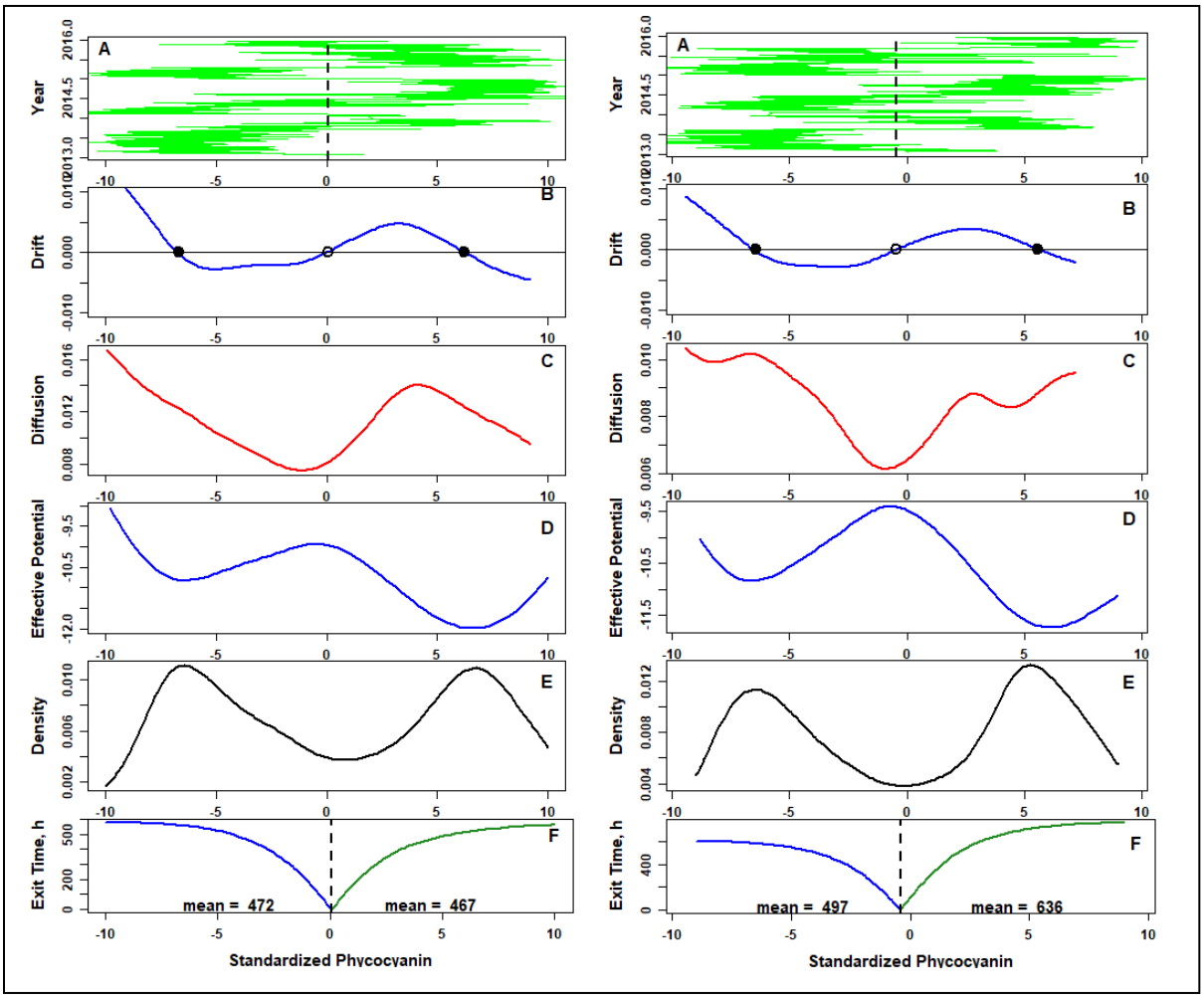

References

Arani, B. M. S., S. R. Carpenter, L. Lahti, E. H. van Nes, and M. Scheffer. 2021. Exit time as a measure of ecological resilience. Science **372:** eaay4895.10.1126/science.aay4895

Bade, D. L., and J. J. Cole. 2006. Impact of chemically enhanced diffusion on dissolved inorganic carbon stable isotopes in a fertilized lake. Journal of Geophysical Research: Oceans **111**.https://doi.org/10.1029/2004JC002684

Carpenter, S., and R. Lathrop. 2014. Phosphorus loading, transport and concentrations in a lake chain: a probabilistic model to compare management options. Aquat Sci **76:** 145-154.10.1007/s00027-013-0324-5

Carpenter, S. R. 2022a. Bootstrap mean exit time: Example for Peter Lake 2013-2015. Zenodo.https://doi.org/10.5281/zenodo.6569548

Carpenter, S. R. 2022b. Chlorophyll dynamics: model of response to DOC, grazing, and phosphorus. Zenodo.https://doi.org/10.5281/zenodo.6568114

Carpenter, S. R. 2022c. Eigenvalues of multivariate autoregression models versus time. Zenodo.https://doi.org/10.5281/zenodo.6522653

Carpenter, S. R., and B. M. S. Arani. 2021. Exit and survival time: New standard scripts. Zenodo.https://doi.org/10.5281/zenodo.6544226

Carpenter, S. R., B. M. S. Arani, E. H. Van Nes, M. Scheffer, and M. L. Pace. 2022. Resilience of phytoplankton dynamics to trophic cascades and nutrient enrichment. Limnology and Oceanography **67:** S258-S265.https://doi.org/10.1002/lno.11913

Carpenter, S. R., and W. A. Brock. 2006. Rising variance: a leading indicator of ecological transition. Ecology Letters **9:** 311-318.DOI 10.1111/j.1461-0248.2005.00877.x

---. 2011. Early warnings of unknown nonlinear shifts: a nonparametric approach. Ecology **92:** 2196-2201.10.1890/11-0716.1

Carpenter, S. R. and others 2001. Trophic cascades, nutrients and lake productivity: Whole-lake experiments. Ecological Monographs **71:** 163-186.doi:10.1890/0012-9615(2001)071[0163:TCNALP]2.0.CO;2

Carpenter, S. R., J. J. Cole, J. F. Kitchell, and M. L. Pace. 1998. Impact of dissolved organic carbon, phosphorus and grazing on phytoplankton biomass and production in lakes. Limnology and Oceanography **43:** 73-80.

Carpenter, S. R., J. J. Cole, M. L. Pace, and G. M. Wilkinson. 2016. Response of plankton to nutrients, planktivory and terrestrial organic matter: a model analysis of whole-lake experiments. Ecology Letters **19:** 230-239.10.1111/ele.12558

Carpenter, S. R., J. F. Kitchell, J. J. Cole, and L. Pace Michael. 2017a. Cascade Project at North Temperate Lakes LTER Core Data Carbon 1984-2016. Environmental Data Initiative.https://doi.org/10.6073/pasta/8d71e8d3fdec619807e5c05fa1b3eb13

---. 2017b. Cascade Project at North Temperate Lakes LTER: Core Data Nutrients 1991-2016. Environmental Data Initiative.https://doi.org/10.6073/pasta/f2956422d5797c61fe6ceb15faa19f3b

Carpenter, S. R., and M. L. Pace. 2018. Synthesis of a 33-yr series of whole-lake experiments: Effects of nutrients, grazers, and precipitation-driven water color on chlorophyll. Limnology and Oceanography Letters **3:** 419-427.doi:10.1002/lol2.10094

Carpenter, S. R., and M. L. Pace. 2022a. DOC, TP, TN of Peter and Tuesday Lakes, Unenriched Years 2003-2021. Zenodo.https://doi.org/10.5281/zenodo.6607788

---. 2022b. Prediction of mixed layer depth from DOC and phosphorus input rate. Zenodo.https://doi.org/10.5281/zenodo.6568103

Draper, N., and H. Smith. 1981. Applied Regression Analysis, 2 ed. John Wiley & Sons.
Gardiner, C. 2009. Stochastic Methods, Fourth ed. Springer.
Hassanibesheli, F., N. Boers, and J. Kurths. 2020. Reconstructing complex system dynamics from time series: a method comparison. New Journal of Physics **22:** 073053.10.1088/1367-2630/ab9ce5
Hilborn, R., and M. Mangel. 1997. The Ecological Detective. Princeton University Press.
Horsthemke, W., and R. Lefever. 1984. Noise-Induced Transitions: Theory and Applications in Physics, Chemistry and Biology. Springer-Verlag.
Ives, A. R., and V. Dakos. 2012. Detecting dynamical changes in nonlinear time series using locally linear state-space models. Ecosphere **3:** art58.10.1890/es11-00347.1
Ives, A. R., B. Dennis, K. L. Cottingham, and S. R. Carpenter. 2003. Estimating community stability and ecological interactions from time-series data Ecological Monographs **73:** 301-330.doi:10.1890/0012-9615(2003)073[0301:ECSAEI]2.0.CO;2
Jones, I., G. George, and C. S. Reynolds. 2005. Quantifying effects of phytoplankton on the heat budgets of two large limnetic enclosures. Freshwater Biology **50:** 1239-1247.https://doi.org/10.1111/j.1365-2427.2005.01397.x
Kling, G. W. 1988. Comparative transparency, depth of mixing, and stability of stratification in lakes of Cameroon, West Africa1. Limnology and Oceanography **33:** 27-40.https://doi.org/10.4319/lo.1988.33.1.0027
Pace, M. L., J. J. Cole, and S. R. Carpenter. 2020. Cascade project at North Temperate Lakes LTER - High Frequency Data for Whole Lake Nutrient Additions 2013-2015 Environmental Data Initiative.https://doi.org/10.6073/pasta/cbe19041db41e720d84970f43156c042
Pole, A., M. West, and J. Harrison. 1994. Applied Bayesian forecasting and time series analysis. Chapman & Hall.
Rinke, K., P. Yeates, and K. O. Rothhaupt. 2010. A simulation study of the feedback of phytoplankton on thermal structure via light extinction. Freshwater Biology **55:** 1674-1693.https://doi.org/10.1111/j.1365-2427.2010.02401.x
Rinn, P., P. G. Lind, M. Wachter, and J. Peinke. 2016. The Langevin approach: an R package for modeling Markov processes. Journal of Open Research Software **4:** e34.DOI: http://doi.org/10.5334/jors.123
Scheffer, M., S. R. Carpenter, V. Dakos, and E. H. van Nes. 2015. Generic Indicators of Ecological Resilience: Inferring the Chance of a Critical Transition. Annual Review of Ecology, Evolution, and Systematics **46:** 145-167.doi:10.1146/annurev-ecolsys-112414-054242
Scheffer, M., E. H. van Nes, M. Holmgren, and T. Hughes. 2008. Pulse-Driven Loss of Top-Down Control: The Critical-Rate Hypothesis. Ecosystems **11:** 226-237.10.1007/s10021-007-9118-8
Tabar, M. R. R. 2019. Analysis and Data-Based Reconstruction of Complex Nonlinear Dynamical Systems. Springer Nature.
West, M., and P. J. Harrison. 1989. Bayesian Forecasting and Dynamic Models. Springer-Verlag.